ACS OMEGA

Open Access



http://pubs.acs.org/journal/acsodf

Article

# A Modular Approach to Obtain HER2-Targeting DM1-Loaded Nanoparticles for Gastric Cancer Therapy

Hui Zhang, Lijiao Guo, Xue Li, Hongtao Liu, Zibin Zhao, Guangling Ji, Yue Huang,* and Xiaodong Wang*

Cite This: *ACS Omega* 2024, 9, 48598−48606

Read Online

ACCESS | Metrics & More | Article Recommendations

**ABSTRACT:** Antibody-based tumor-targeting nanomedicines, despite their high efficacy, present significant challenges in preparation and long-term storage. We introduce a novel approach for the synthesis of durable, ready-to-use, antibody-coupled nanomedical drugs. Our research centers on the development of HER2-targeting DM1-loaded nanoparticles for gastric cancer treatment using a modular methodology. We synthesized Fc-PLG-Mal, conjugated DM1 through a "click" reaction, and subsequently bound the resultant compound with the HER2 antibody trastuzumab. The nanoparticles demonstrated a high drug loading content, stable particle size, and effective HER2 targeting. HER2-PLG-DM1 exhibited significant cytotoxicity against NCI-N87 gastric cancer cells, with an $IC_{50}$ of 0.35 nM. Biodistribution revealed rapid and substantial tumor accumulation, 6-fold higher than that of nontargeting IgG-PLG-DM1. HER2-PLG-DM1 significantly inhibited tumor growth in NCI-N87 tumor-bearing mice, achieving a 90.8% tumor inhibition rate, and displayed dose-dependent effects without significant liver and kidney toxicity. These studies offer an efficient and stable method for the preparation of antibody-coupled drugs.

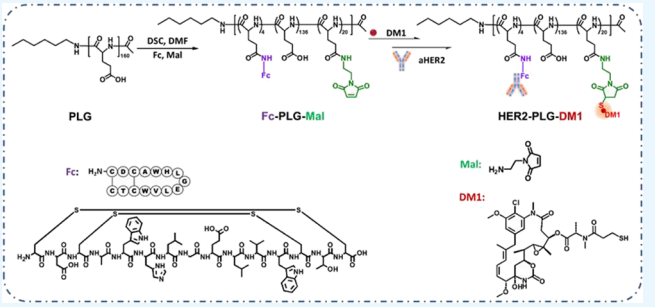


## 1. INTRODUCTION

Passive targeting anticancer preparations (PTAPs) opened the gate for tumor-targeted therapy, generally by taking advantage of the enhanced permeability and retention effect (EPR) of tumor tissues.[1−5] Normally, PTAPs contained antineoplastic drugs and unmodified carriers, referring to nanoparticles, liposomes, and polymer micelles.[6−10] The accumulation of antineoplastic drugs toward tumor tissues was based on the indistinctive uptake of immune cells and EPR of tumors to these microparticles.[11] However, more accurate targeting ability of PTAPs was limited by their carrier properties, such as grain size, zeta potential, and compound composition, especially the lack of targeted modifying carriers that could target tumor tissue actively.

Active targeting anticancer preparations (ATAPs) mainly include small molecule targeting agents, monoclonal antibodies, antibody-drug conjugates (ADCs), and targeted nanodrug delivery systems (TNDSs).[12] Many researchers focus on the investigation of ADCs and TNDSs.[13−18] ADCs deliver potent cytotoxic compounds selectively to tumor cells by conjugating them to antibodies, thus improving the therapeutic effect of chemotherapeutic agents. The basic constituents of ADCs are antibodies, cytotoxic compounds, and the linkers.[19] By now, nine ADCs are currently approved for cancer treatment, with many more of them being tested in preclinical and clinical studies.[20] This has spurred tremendous research interests in the field.[21−25] It is recognized that many nanocarriers, including natural and chemical synthesis products, could be used as targeted deliver systems for TNDS.[26−28] Tian and colleagues designed an antibody-modified prodrug nanoparticle based on biomacromolecule dextran (DEX) for the efficient delivery of the anticancer drug doxorubicin (DOX). The team combined oxidized dextran (ODEX) with DOX through a Schiff base reaction to form ODEX-DOX, which could self-assemble into nanoparticles (NPs). Furthermore, they prepared acid-responsive and antibody-modified CD147-ODEX-DOX NPs by reacting CD147 monoclonal antibodies with aldehyde groups on the surface of the ODEX-DOX NPs. These nanoparticles have a small particle size and a high DOX loading capacity. They demonstrated good stability and pH responsiveness in various media and tumor microenvironments. *In vitro* and *in vivo* experiments had shown that CD147-ODEX-DOX NPs can significantly inhibit the growth of

**Received:** August 17, 2024
**Revised:** November 10, 2024
**Accepted:** November 18, 2024
**Published:** November 22, 2024

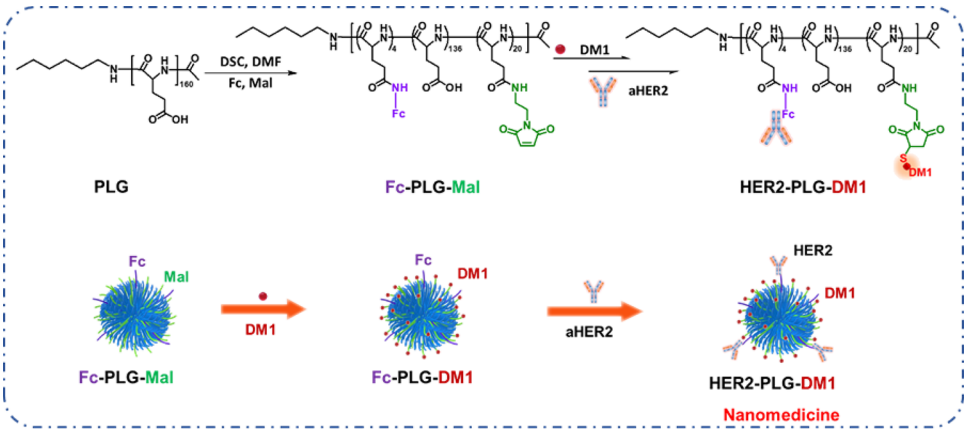


**Figure 1.** Synthetic route of HER2-PLG-DM1.

HepG2 tumors.[29] Lehot et al. developed antibody-toxic nanoparticle conjugates (ATNPs) by complexing anti-HER2 antibody-oligonucleotide conjugates (AOCs) with cytotoxic cationic polydiacetylenic micelles. The optimizing ATNPs were found to selectively kill antigen-positive SKBR-2 cells *in vitro* and perform 60% tumor regression *in vivo*.[30] Therefore, ATAPs are a classical and efficient cancer therapy strategy.

However, the current technology of ATAP preparation is complicated and time-consuming, and the inactivation and off-target phenomena also cannot be neglected during the preparation process. Herein, we report on the development of a novel HER2-targeted nanomedicine loaded with DM1, relying on a simple and quick method. As outlined in Figure 1, we utilized the carboxyl groups on the side chain of azide-terminated poly(L-glutamic acid) (PLG) as the payload binding sites to achieve the nanomedicine. We first grafted *N*-(2-aminoethyl)maleimide hydrochloride (Mal-$C_2H_4$-$NH_2$·HCl) onto the carboxyl group of PLG to introduce maleimide groups, forming PLG-Mal. The Fc-III-4C peptide-PLG-Mal (Fc-PLG-Mal) was prepared through an amide reaction between the carboxyl group and amido group of the Fc-III-4C peptide. The mentioned Fc-III-4C peptide exhibits a strong affinity to the Fc segment of IgG of various species, especially the human IgG that has the largest binding affinity ($K_D$ = 2.45 nM). Subsequently, a thiol-maleimide "click" chemistry approach was utilized, involving the reaction between the maleimide group and the sulfhydryl group of DM1, to synthesize Fc-PLG-DM1.[31] The HER2-PLG-DM1 conjugate was then prepared by simply mixing the antibody with Fc-PLG-DM1 in an aqueous solution for a brief period of 2 h. This process leveraged the strong binding affinity between the Fc-III-4C peptide and the Fc region of the HER2 antibody. Our preparation method was simple and quick, benefiting form the "click" reaction of thiol-maleimide and the affinity ability of the Fc-III-4C peptide. In addition, HER2-PLG-DM1 showed significant tumor inhibition effects, with a tumor suppression rate of 90.8%, and the therapeutic effect of nanomedicine groups was significantly better than that of mere mixture groups. In the previous study,[32] to increase the DAR value, the material preparation process involved five types of conjugations (maleimide conjugation with PLG, DBCO-PEG-NHS conjugation with the Fc-III-4C peptide, thiol conjugation on DM1 with maleimide, azide with DBCO click reaction, and Fc-III-4C peptide conjugation with an antibody). In this study, we directly conjugated the Fc-III-4C peptide onto PLG, avoiding the conjugation of DBCO-PEG-NHS with the Fc-III-4C peptide and the click reaction between azide and DBCO. The successful formulation of HER2-PLG-DM1 illustrates the promising potential of this strategy for the future design and development of functional nanomedicines.

## 2. MATERIALS AND METHODS

**2.1. Materials.** γ-Benzyl-L-glutamate-*N*-carboxyanhydride (BLG-NCA) was procured from Chengdu Enlai Biological Technology Co., Ltd., China. The crude material was subjected to a double recrystallization process using ethyl acetate and subsequently dried under vacuum conditions at ambient temperature before being utilized. *N*,*N*′-Disuccinimidyl carbonate (DSC) was obtained from Shanghai Bidepharmatech Co., Ltd. *N*-(2-Aminoethyl)maleimide hydrochloride salt was supplied by Leyan Co., Ltd. Fc-III-4C peptide was purchased from Shanghai GL Biochem Ltd. Cyanine 5 amine (Cy5-$NH_2$) was obtained from Xi'an Qiyue Biotechnology Co., Ltd. Anti-human HER2 monoclonal antibody (trastuzumab) was purchased from Bioxcell Co., Ltd. RPMI 1640 medium, fetal bovine serum (FBS), and phosphate-buffered saline (PBS) were supplied by Dalian Meilun Biotechnology Co., Ltd. Penicillin and streptomycin were purchased from Beijing Sevenbio Co., Ltd. The Cell Counting Kit-8 (CCK-8) assay was sourced from Solarbio Co., Ltd. All additional reagents and solvents were acquired from Sinopharm Chemical Reagent Co., Ltd., and employed without further purification.

**2.2. Cells and Animals.** The NCI-N87 gastric cancer cell line was obtained from the BeNa Culture Collection Co., Ltd., China, and cultured in RPMI 1640 medium supplemented with 10% FBS and 1% penicillin−streptomycin solution at 37 °C under 5% $CO_2$. Female BALB/c nude mice (6−8 weeks old, 15−19 g) were purchased from Beijing Vital River Laboratory Animal Technology Co., Ltd. All animals received proper care, and the *in vivo* studies were conducted according to the guidelines approved by the Institutional Animal Care and Use Committee of Changchun Institute of Applied Chemistry, Chinese Academy of Sciences.

To establish a subcutaneous gastric cancer model, an inoculum size of 5 × $10^6$ NCI-N87 cells was subcutaneously injected into the right flank of BALB/c nude mice.[33] When the tumor volume was approximately 100 $mm^3$, the mice were randomly divided into needed groups ($n$ = 5) and treated with a designed dose and frequency.

**2.3. Instruments and Methods.** The $^1$H NMR spectra of products were recorded on an AV-300 spectrometer (Bruker)



https://doi.org/10.1021/acsomega.4c07442
ACS Omega 2024, 9, 48598−48606

at room temperature in deuterated sodium hydroxide (NaOD)/$D_2O$. Dynamic light scattering (DLS) and zeta potential data were measured by a zeta potential/size analyzer (Malvern, Nano-ZS, UK). The transmission electron microscopy (TEM) test (JEM-1400Flash, 120 kV, Japan) was carried out to investigate the morphology features of the products. The loading content of maytansine (DM1) was quantified by an ultraviolet/visible light spectroscopy test (UV/vis Lambda 365 spectrometer, PerkinElmer, USA). The cell viability assay experiment was carried out with a microplate reader (Tecan Spark multimode microplate reader, Swiss). The biodistribution analysis of products was measured using an IVIS lumina LT series III *in vivo* imaging system (PerkinElmer, USA).

**2.4. Preparation of Fc-PLG-Mal, HER2-PLG-DM1, Fc-PLG-DM1/Cy5, HER2-PLG-DM1/Cy5, and IgG-PLG-DM1/Cy5.** Fc-PLG-Mal was synthesized via a one-pot method. PLG (210.0 mg, 10.0 $\mu$mol) was dissolved in 8.0 mL of anhydrous *N*,*N*-dimethylformamide (DMF). Then, TEA (40.8 mg, 0.4 mmol) and DSC (76.8 mg, 0.3 mmol) were added and reacted at room temperature for 12 h. Subsequently, the Fc-III-4C peptide (69.4 mg, 40.0 nmol) was introduced into the prepared solution. The mixture was stirred at ambient temperature to allow the reaction to proceed for 24 h. Following this, maleimide (38.8 mg, 0.4 mmol) was incorporated into the solution, which was then continuously stirred at room temperature for an additional 48 h. It is critical to protect the reaction mixture from exposure to water and oxygen during this process. After that, the DMF solution was precipitated by using an excess amount of distilled water in the dialysis membrane (MWCO = 3500 Da) to obtain Fc-PLG-Mal. Fc-PLG-Mal (144 mg, 4.0 $\mu$mol) was dissolved in 5 mL anhydrous DMF, and then DM1 (214.5 mg, 0.2 mmol) dissolved in acetonitrile was added into the DMF solution. After a short time of ultraviolet radiation, the mixture solution was transferred into a dialysis membrane (MWCO = 7000 Da) and dialyzed against distilled water to gain Fc-PLG-DM1. The drug loading content (DLC) of DM1 was determined by using UV/vis spectroscopy. For the preparation of HER2-PLG-DM1, trastuzumab, which is the HER2 antibody, was mixed with Fc-PLG-DM1 in phosphate-buffered saline (PBS) at a pH of 7.4 for a brief period of 2 h. This process capitalizes on the strong affinity between the Fc-III-4C peptide and the crystallizable fragment (Fc) of trastuzumab. The synthesis route of HER2-PLG-DM1 is presented in Figure 1.

Similarly, this method was also used to prepare Fc-PLG-DM1/Cy5, HER2-PLG-DM1/Cy5, and IgG-PLG-DM1/Cy5. Fc-PLG-Mal (144 mg, 4.0 $\mu$mol) was dissolved in 5 mL of anhydrous DMF, and then DM1 (214.5 mg, 0.2 mmol) and fluorescent dyes [Cyanine 5 amine (Cy5-$NH_2$, 8.0 mg, 12.2 $\mu$mol) dissolved in acetonitrile were added into the DMF solution, and the mixture was allowed to react for 48 h. The reaction solution was transferred into a dialysis membrane (MWCO = 7000 Da) and dialyzed against distilled water to obtain Fc-PLG-DM1/Cy5. The Cy5 loading content was measured by UV−vis spectroscopy.

Because of the strong binding affinity of the Fc-III-4C peptide for the Fc region of monoclonal antibodies, simple mixing and stirring of the monoclonal antibodies (Trastuzumab and IgG) with Fc-PLG-DM1/Cy5 in solution are sufficient to yield the conjugates HER2-PLG-DM1/Cy5 and IgG-PLG-DM1/Cy5. Fc-PLG-DM1/Cy5 (100.0 nmol) and monoclonal antibodies (HER2: 50.0 nmol, IgG: 50.0 nmol) were dissolved and stirred in 1.0 mL of PBS buffer (pH 7.4) for 2 h. The hydrodynamic size and zeta potential were determined with a Malvern potential/size analyzer.

**2.5. Cell Viability Assay.** The cytotoxicity of IgG-PLG-DM1 and HER2-PLG-DM1 was evaluated using a CCK-8 assay.[34] Typically, NCI-N87 cells were seeded in 96-well plates at a density of $5 \times 10^3$ cells per well and incubated overnight. IgG-PLG-DM1 and HER2-PLG-DM1 were added at the designed concentrations. After 48 h of incubation, 20.0 $\mu$L of the CCK-8 solution was added into each well, and the wells were incubated for 1 h. The absorbance of each well was measured at 450 nm using a microplate reader (Tecan Spark multimode microplate reader, Switzerland) to determine the cell viability.

**2.6. Biodistribution Analysis.** NCI-N87 tumor-bearing BALB/c nude mice were used for biodistribution analysis.[35] The mice were treated with HER2-PLG-DM1/Cy5 or IgG-PLG-DM1/Cy5 at matched Cy5 fluorescence content. Next, 1, 4, and 12 h postinjection, one mouse from each group was sacrificed. The main organs and tumors were collected and analyzed using an IVIS Lumina LT Series III *in vivo* imaging system.

**2.7. *In Vivo* Antitumor Efficacy.** BALB/c nude mice (female, 6−8 weeks) were subcutaneously injected with NCI-N87 cells in the right flank to establish a subcutaneous NCI-N87 tumor-bearing model.[36] When the tumor volumes were approximately 100 $mm^3$, the mice were randomly divided into five groups ($n$ = 5) and treated with PBS, HER2 + IgG-PLG-DM1 (2.17 mg/kg HER2, 2.31 mg/kg IgG, and 0.08 mg/kg DM1), HER2*2 + IgG-PLG-DM1*2 (2.17 mg/kg HER2, 2.31 mg/kg IgG, and 0.08 mg/kg DM1), HER2-PLG-DM1 (1.09 mg/kg HER2 and 0.04 mg/kg DM1), and HER2-PLG-DM1*2 (2.17 mg/kg HER2 and 0.08 mg/kg DM1). Therapeutic treatments were given at 6 day intervals for a total of three administrations. Tumor growth and body weight were assessed every 3 days over a 27 day period. The formula used to calculate the tumor volume was as follows:

$$\text{tumor volume } (V) = a \times b^2/2$$

where $a$ and $b$ stand for the longest and shortest diameters of the tumors measured with Vernier calipers. The tumor inhibition rate ($E$) was calculated by the following formula:

$$E_s = \left(1 - \frac{TV_s - T_0}{TV_c - T_0}\right) \times 100\%$$

where $TV_s$ and $TV_c$ are the average tumor volumes of the sample and control group, respectively. $T_0$ is the initial average tumor volume on day 0.

**2.8. Systemic Toxicity Evaluation *In Vivo*.** Blood was collected from mice ($n$ = 5) after various treatments for the analysis of serum biochemical parameters. Liver function parameters (alanine aminotransferase (ALT) and aspartate aminotransferase (AST)) and kidney function parameters (blood urea nitrogen (BUN) and uric acid (UA)) were measured following the manufacturer's instructions.

**2.9. Hematoxylin and Eosin (H&E) Staining.** From BALB/c nude mice, the principal organs, including the heart, liver, spleen, lungs, and kidneys, as well as the tumor were harvested and immersed in 4% buffered paraformaldehyde for a duration of 24 h for fixation.[37] Subsequently, these tissues were embedded in paraffin, sectioned to a thickness of 5.0 $\mu$m, and stained with hematoxylin and eosin (H&E) to micro-


https://doi.org/10.1021/acsomega.4c07442
ACS Omega 2024, 9, 48598−48606

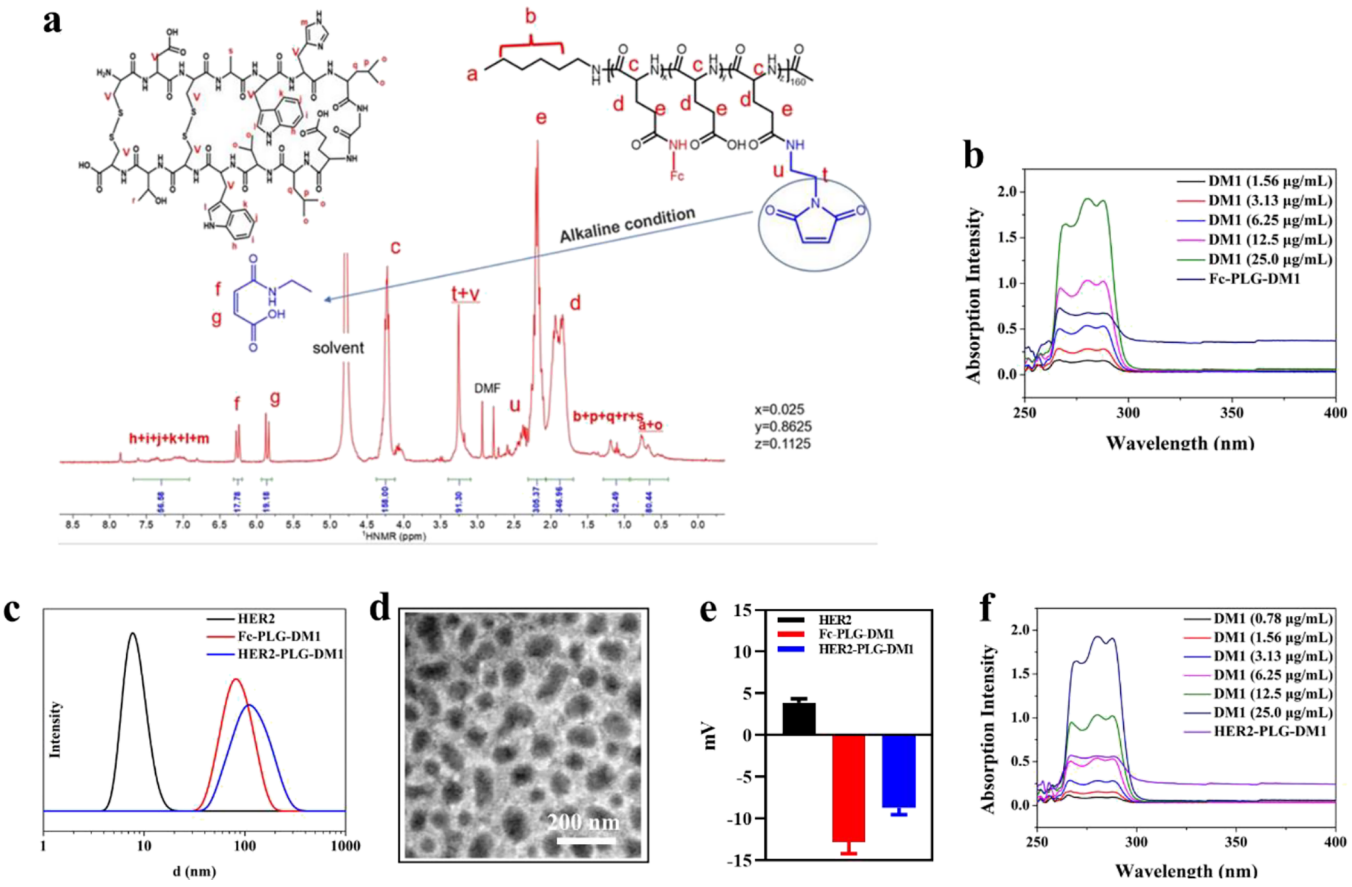


**Figure 2.** (a) $^1$H NMR spectrum of Fc-PLG-Mal. (b) UV/vis spectra of DM1 and Fc-PLG-DM1. (c) Diameters of trastuzumab (HER2), Fc-PLG-DM1, and HER2-PLG-DM1. (d) The transmission electron microscopy (TEM) images of HER2-PLG-DM1. (e) The zeta potentials of trastuzumab, Fc-PLG-DM1, and HER2-PLG-DM1. (f) UV/vis spectroscopy of DM1 and HER2-PLG-DM1.

scopically assess histopathological alterations (Nikon TE 2000U microscope).

**2.10. Statistical Analysis.** Data are presented as the mean ± standard deviation (SD). The statistical significance of differences was evaluated using a one-way analysis of variance (ANOVA). A difference was considered statistically significant for values of $P < 0.05$ and highly significant for values of $P < 0.01$.

## 3. RESULTS AND DISCUSSION

**3.1. Characterization of Fc-PLG-Mal and HER2-PLG-DM1.** To enable quick bonding of the DM1 and antibody to the side chain of PLG, aminol groups of Mal-$C_2H_4$-$NH_2$·HCl and Fc-III-4C were used to react with −COOH on the side chain of PLG, resulting in the formation of Fc-PLG-Mal. Figure 2a shows the $^1$H NMR spectrum of Fc-PLG-Mal. The Fc-PLG-DM1 preparation was started with a "click" chemical reaction between the maleimide group and the sulfhydryl group of DM1 in the DMF solution. Then, the DMF solution underwent dialysis (with a molecular weight cutoff of 3500) against distilled water followed by freeze-drying to yield the Fc-PLG-DM1 product. The presence of peaks f at $\delta$ 6.30 ppm and g at $\delta$ 5.86 ppm in the spectroscopic analysis indicated the ring opening of the maleimide group under alkaline conditions. The ratio of peak areas for peaks a, h, and i was 12:51:51, indicating a mean number of 20 maleimide groups grafted to one PLG chain. Meanwhile, the DM1 loading content (DLC) contained in Fc-PLG-DM1 was measured by ultraviolet/visible light (UV/vis) spectroscopy (Figure 2b). Subsequently, we prepared HER2-PLG-DM1 by mixing the HER2 antibody with Fc-PLG-DM1 in PBS (pH 7.4) for only 2 h, taking advantage of the high-affinity interaction between the Fc-III-4C peptide and Fc segment of the antibody. As shown in Figure 2c, the mean diameters of trastuzumab, Fc-PLG-DM1, and HER2-PLG-DM1 measured by the dynamic light scattering (DLS) were 7.7 ± 1.2 nm (polydispersity index [PDI] = 0.10), 82.3 ± 5.8 nm (PDI = 0.21), and 112.3 ± 12.5 nm (PDI = 0.28), respectively. Moreover, the absence of any free monoclonal antibodies in the particle size distribution curve confirms the successful conjugation of trastuzumab to Fc-PLG-DM1. Figure 2d shows the transmission electron microscopy (TEM) images that the mean diameter of HER2-PLG-DM1 was approximately 90.0 ± 10.5 nm. The zeta potentials of trastuzumab, Fc-PLG-DM1, and HER2-PLG-DM1 were 3.87 ± 0.5, −12.8 ± 1.4, and −8.74 ± 0.8 mV, respectively (Figure 2e). The negative charges were attributed to the presence of carboxyl groups on the side chain of PLG. The DLC of HER2-PLG-DM1 was measured by UV/vis spectroscopy (Figure 2f) and was found to be 5.74 ± 0.08%. Finally, IgG-PLG-DM1, HER2-PLG-DM1/Cy5, and IgG-PLG-DM1/Cy5 were prepared using the same method.

**3.2. *In Vitro* Cytotoxicity Assay and Biodistribution Analysis.** The cytotoxicity of IgG-PLG-DM1 and HER2-PLG-DM1 against NCI-N87 cells (Figure 3a) was measured by the CCK-8 assay. As shown in Figure 3a, HER2-PLG-DM1 demonstrated significant cytotoxicity toward NCI-N87 cells


https://doi.org/10.1021/acsomega.4c07442
ACS Omega 2024, 9, 48598−48606

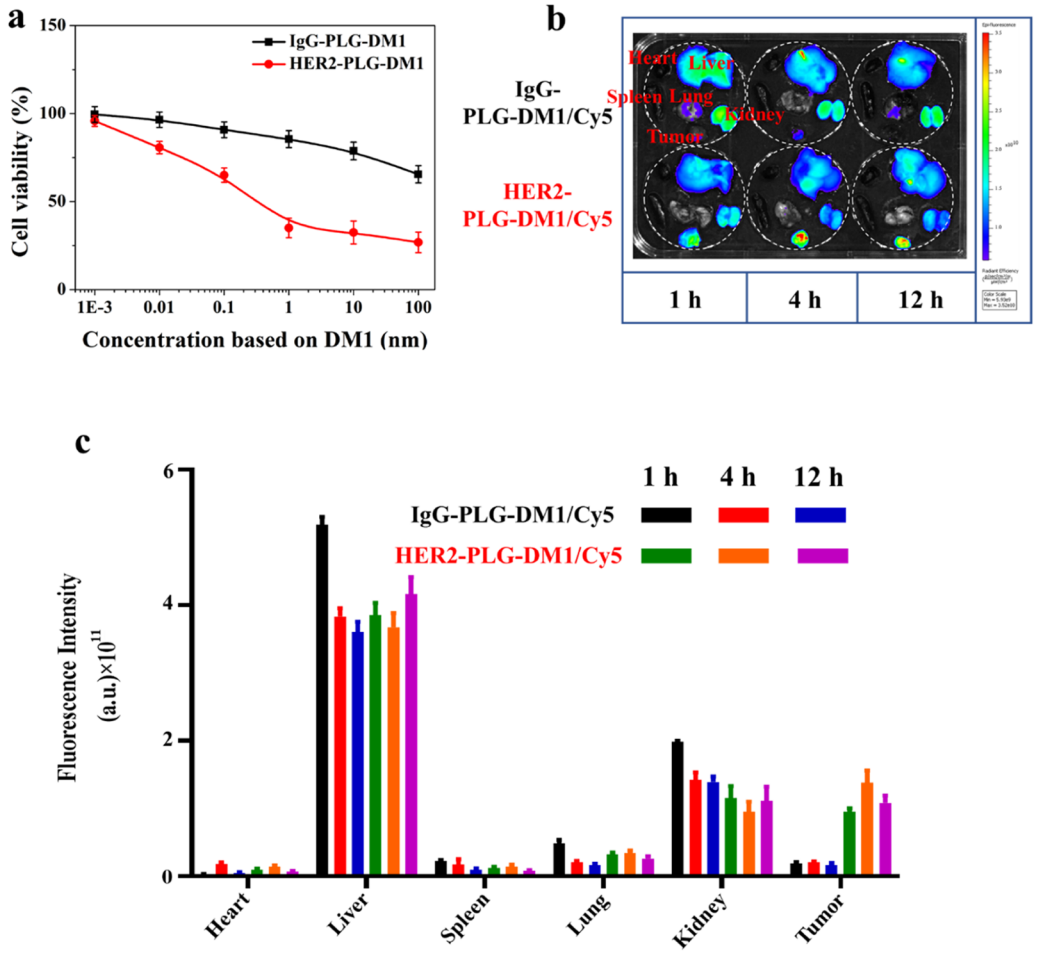


**Figure 3.** (a) Cytotoxicity of IgG-PLG-DM1 and HER2-PLG-DM1. (b) *Ex vivo* imaging of IgG-PLG-DM1/Cy5 and HER2-PLG-DM1/Cy5 in different tissues after 1, 4, and 12 h. (c) Quantitative fluorescence analysis of different tissues after 1, 4, and 12 h ($n$ = 3).

after 72 h of incubation. The $IC_{50}$ value of HER2-PLG-DM1 was 0.35 nM. The cytotoxicity of IgG-PLG-DM1 was relatively lower than that of HER2-PLG-DM1, as evidenced by $IC_{50}$ higher than 100 nM. The improved delivery efficiency of HER2-PLG-DM1 toward NCI-N87 cells with high HER2 expression may be attributed to the HER2-targeting antibody (trastuzumab) that allows HER2-PLG-DM1 to reach NCI-N87 cells efficiently. The much lower cytotoxicity of IgG-PLG-DM1 toward NCI-N87 may be due to the nontargeting IgG and PLG segments that block the direct uptake of NCI-N87 cells to DM1.

Biodistribution of HER2-PLG-DM1 in BALB/c nude mice was measured by fluorescence imaging. Figure 3b shows the fluorescence images of main organs and tumors of female nude mice at intervals of 1, 4, and 12 h after injection by IgG-PLG-DM1/Cy5 and HER2-PLG-DM1/Cy5. IgG-PLG-DM1/Cy5 nanoparticles were predominantly found in the liver and kidneys, with minimal accumulation at the tumor site over time. In stark contrast, a rapid and substantial accumulation of HER2-PLG-DM1/Cy5 within the tumor was observed, reaching a peak within just 4 h postadministration. This selective targeting underscores the potential of HER2-PLG-DM1/Cy5 as a theranostic agent for HER2-positive tumors, highlighting its utility in both diagnostic imaging and targeted drug delivery. In addition, much more tumor accumulation of HER2-PLG-DM1/Cy5 than IgG-PLG-DM1/Cy5 group at 12 h was still observed. Figure 3c shows the fluorescence intensity of main organs and tumors at different times. Liver and kidneys are the main metabolic organs of IgG-PLG-DM1 and HER2-PLG-DM1. After 1 h administration, the fluorescence intensity in tumors of HER2-PLG-DM1/Cy5 was 4.1-fold greater than that observed in tumors of IgGPLG-DM1/Cy5 and then 6.0-fold at 4 h, and a consistently high intensity was maintained after 12 h. These results indicated that HER2-PLG-DM1 could recognize and accumulate at NCI-N87 tumor sites, therefore improving the targeting ability and reducing the potential side effects.

**3.3. *In Vivo* Inhibition Tumor Tests.** The effectiveness of HER2-PLG-DM1 in treating tumors was evaluated in nude mice with NCI-N87 tumors. When the tumors reach approximately 100 $mm^3$, the mice were divided randomly into five groups ($n$ = 5) and treated on days 0, 6, and 12 via tail vein injection as follows: PBS, aHER2 + IgG-PLG-DM1 (2.17 mg/kg of HER2, 2.31 mg/kg of IgG, and 0.08 mg/kg of DM1), aHER2*2 + IgG-PLG-DM1*2 (2.17 mg/kg of HER2, 2.31 mg/kg of IgG, and 0.08 mg/kg of DM1), HER2-PLG-DM1 (1.09 mg/kg of HER2 and 0.04 mg/kg of DM1), and HER2-PLG-DM1*2 (2.17 mg/kg of HER2 and 0.08 mg/kg of DM1) (Figure 4a). Figure 4b,c depicts the tumor growth and the corresponding change in weight of the mice across all groups under study. Compared to the PBS group, HER2-PLG-DM1 and HER2-PLG-DM1*2 exhibit a significant inhibition effect, with tumor growth inhibition values of 79.5 and 90.8% on day 27. HER2-PLG-DM1 showed a dose-dependence


https://doi.org/10.1021/acsomega.4c07442
ACS Omega 2024, 9, 48598−48606

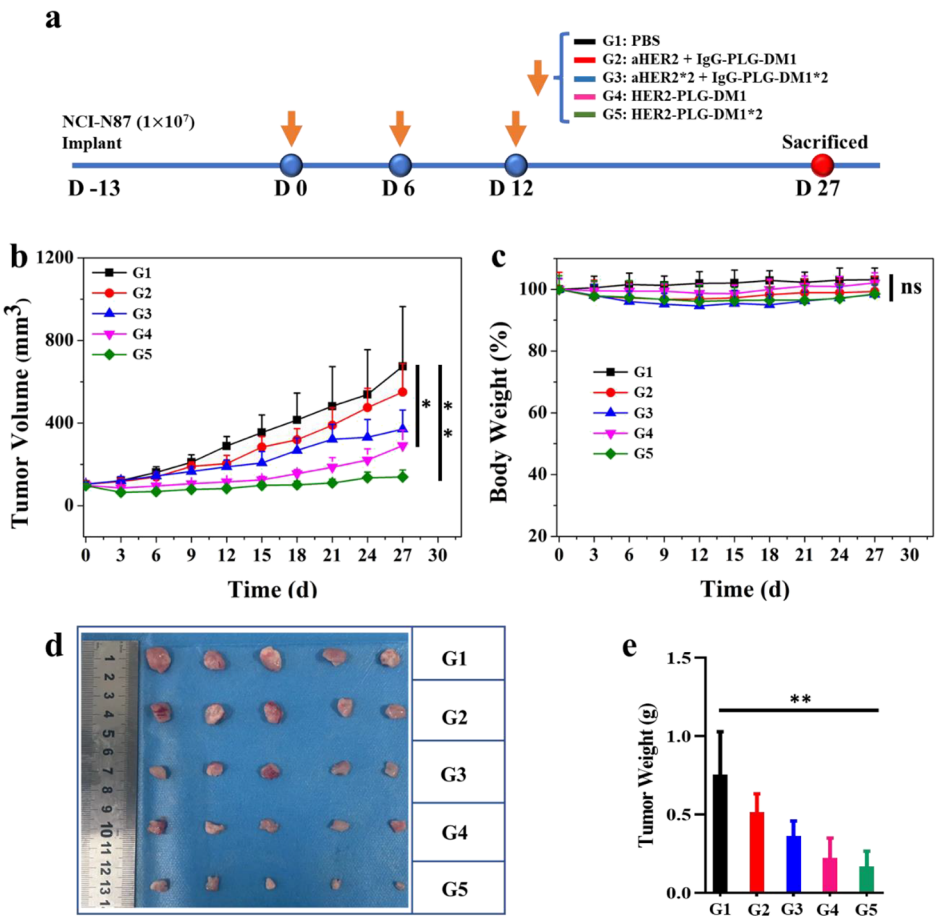


**Figure 4.** Pharmacodynamic results of the designed groups on NCI-N87-bearing mice. Therapy regimen (a), mean tumor size (b), body weight (c), tumor images (d), and tumor weight (e) ($n$ = 5). Data are presented as means ± SD. *$P$ < 0.05 and **$P$ < 0.01.

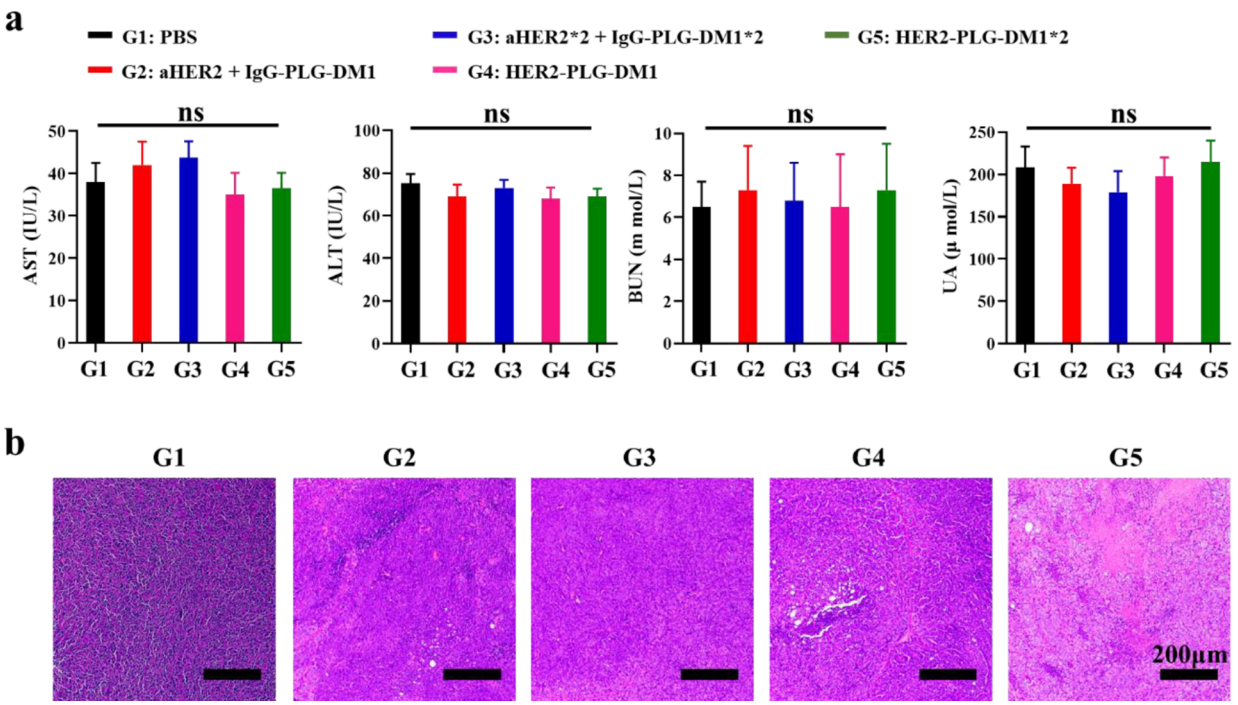


**Figure 5.** (a) Hepatorenal function index and (b) H&E analysis of designed groups. Data are presented as means ± SD.

relationship. Furthermore, HER2-PLG-DM1 groups also showed significantly improved antitumor ability toward aHER2 + IgG-PLG-DM1 groups. At the equivalent total payload dose, the antitumor efficacy of HER2-PLG-DM1 was



https://doi.org/10.1021/acsomega.4c07442
ACS Omega 2024, 9, 48598−48606

still higher than that of aHER2 + IgG-PLG-DM1, which may be due to the specific binding of trastuzumab to HER2-positiveNCI-N87 cells, which facilitated the delivery of more DM1 from HER2-PLG-DM1 to the tumor. The body weight loss of all groups was less than 10%, which indicates the safety of all drugs at the given dose. The tumor images (Figure 4d) and tumor weight (Figure 4e) of all groups at the end of the experiment period showed that HER2-PLG-DM1 groups possessed a significant anticancer effect on control and mixture groups.

The liver and kidney function tests, as depicted in Figure 5a, indicated no significant alterations in the levels of aspartate aminotransferase (AST), alanine aminotransferase (ALT), blood urea nitrogen (BUN), or uric acid (UA) following the administration of HER2-PLG-DM1. This suggests that the treatment did not cause substantial hepatic or renal toxicity, which is a critical consideration in the assessment of drug safety. The maintenance of these biomarkers within normal ranges post-treatment underscores the potential safety profile of HER2-PLG-DM1 in the context of liver and kidney function. These results confirmed the acceptable cytotoxicity of the DM1-loaded nanomedicine, which is consistent with the body weight change. The therapeutic efficacy of HER2-PLG-DM1 was evaluated by tumor staining with hematoxylin and eosin (H&E) (Figure 5b). Hematoxylin and eosin (H&E) staining is a fundamental method in histopathological analysis, providing crucial morphological details of tumor tissues. In the context of evaluating the effects of treatments like HER2-PLG-DM1 and IgG-PLG-DM1 on tumor growth, H&E staining plays a pivotal role. The pathological analysis of H&E stain sections from the PBS group would typically reveal the robust proliferation of tumor cells, characterized by intact cell morphology, indicating a lack of treatment impact. Conversely, in groups treated with aHER2 + IgG-PLG-DM1, there is a notable reduction in tumor cell density, suggesting a therapeutic effect. In contrast, the tumor morphology of HER2-PLG-DM1 groups became sparse and more isolated, with significant nuclear pyknosis and necrosis than PBS and aHER2 + IgG-PLG-DM1 groups. These results indicated that HER2-PLG-DM1 nanomedicine facilitated more delivery of DM1 to the tumors than PBS control and mixture groups, resulting in the apoptosis of the NCI-N87 tumor cells.

## 4. CONCLUSIONS

In this work, we successfully prepared a nanomedicine sample containing trastuzumab as an active targeting antibody, along with DM1, which exhibits high antitumor efficacy. By utilization of the carboxyl groups in the side chain of the poly(L-glutamic acid) and the amido group of maleimide and Fc-III-4C peptide, Fc-PLG-Mal was synthesized. Then, the "click" reaction between DM1 and maleimide and the stirring operation in aqueous solution were utilized to prepare the active targeting nanomedicine HER2-PLG-DM1 in a very simple and quick manner. The introduction of the Fc-III-4C peptide avoided the chemical impact on the targeting ability of the Fab segment of monoclonal antibodies. The DLS, TEM, zeta potential, and UV/vis tests were carried out to confirm the properties of the nanomedicine HER2-PLG-DM1. In addition, HER2-PLG-DM1 was actively targeted and internalized into HER2-expressing NCI-N87 cells. The biodistribution analysis certified that this active targeting nanomedicine exhibits a 6.0-fold increase in tumor accumulation compared to the nontargeting IgG-PLG-DM1. Furthermore, HER2-PLG-DM1 showed significant antitumor activity with a tumor inhibition rate of 90.8%. This research suggests that HER2-PLG-DM1 has the potential ability to actively target HER2-expressing tumor and be used as an active targeting nanomedicine for HER2-positive gastric cancer therapy.

## AUTHOR INFORMATION


### Corresponding Authors

**Yue Huang** − *Key Laboratory of Polymer Ecomaterials, Changchun Institute of Applied Chemistry, Chinese Academy of Sciences, Changchun 130022, China*; Email: huangyue@ciac.ac.cn

**Xiaodong Wang** − *Gastroenteric Medicine and Digestive Endoscopy Center, The Second Hospital of Jilin University, Changchun, Jilin Province 130041, China*; orcid.org/0000-0001-5924-4649; Email: wangxiaodong@jlu.edu.com

### Authors

**Hui Zhang** − *Department of Clinical Laboratory Medicine, The Affiliated Hospital to Changchun University of Chinese Medicine, Changchun, Jilin Province 130021, China*

**Lijiao Guo** − *Department of Clinical Laboratory Medicine, The Affiliated Hospital to Changchun University of Chinese Medicine, Changchun, Jilin Province 130021, China*

**Xue Li** − *Department of Clinical Laboratory Medicine, The Affiliated Hospital to Changchun University of Chinese Medicine, Changchun, Jilin Province 130021, China*

**Hongtao Liu** − *Jilin Academy of Chinese Medicine Sciences, Changchun, Jilin Province 130117, China*

**Zibin Zhao** − *Jilin Academy of Chinese Medicine Sciences, Changchun, Jilin Province 130117, China*

**Guangling Ji** − *Gastroenteric Medicine and Digestive Endoscopy Center, The Second Hospital of Jilin University, Changchun, Jilin Province 130041, China*

Complete contact information is available at: https://pubs.acs.org/10.1021/acsomega.4c07442


### Author Contributions

Hui Zhang: Writing−original draft, Investigation, Formal analysis, Data curation, Funding acquisition. Lijiao Guo: Validation, Methodology, Formal analysis. Xue Li: Data curation. Hongtao Liu: Methodology. Zibin Zhao: Writing−review and editing, Supervision. Guanglin Ji: Supervision, Formal analysis. Yue Huang: Writing−review and editing. Xiaodong Wang: Writing−review and editing, Conceptualization.


### Funding

This work was supported by the Project of the National Natural Science Foundation of China (52103195) and the Natural Science Foundation of Jilin Province (20210101275JC).


### Notes

The authors declare no competing financial interest.

## ACKNOWLEDGMENTS

We would like to thank the members of the Key Laboratory of Polymer Electronic Materials, Changchun Institute of Applied Chemistry, Chinese Academy of Sciences, for their generous guidance on the chemical synthesis and characterization in this study.



https://doi.org/10.1021/acsomega.4c07442
ACS Omega 2024, 9, 48598−48606

## REFERENCES


(1) Bayón Cordero, L.; Alkorta, I.; Arana, L. Application of Solid Lipid Nanoparticles to Improve the Efficiency of Anticancer Drugs. *Nanomaterials* **2019**, *9* (3), 474.

(2) Kashkooli, F. M.; Soltani, M.; Souri, M.; Meaney, C.; Kohandel, M. Nexus Between In Silico and In Vivo Models to Enhance Clinical Translation of Nanomedicine. *Nanotoday* **2021**, *36*, No. 101057.

(3) Chen, L.; Zheng, J.; Du, J.; Yu, S.; Yang, Y.; Liu, X. Folic acid-conjugated magnetic ordered mesoporous carbon nanospheres for doxorubicin targeting delivery. *Mater. Sci. Eng.: C* **2019**, *104*, No. 109939.

(4) Lin, L.; Wang, Y.; Cai, M.; Jiang, X.; Hu, Y.; Dong, Z.; Yin, D.; Liu, Y.; Yang, S.; Liu, Z.; Zhuang, J.; Xu, Y.; Guo, C. F.; Chang, L. Multimicrochannel Microneedle Microporation Platform for Enhanced Intracellular Drug Delivery. *Adv. Funct. Mater.* **2022**, *32* (21), No. 2109187.

(5) Jin, Z.; Nguyen, K. T.; Go, G.; Kang, B.; Min, H. K.; Kim, S. J.; Kim, Y.; Li, H.; Kim, C. S.; Lee, S.; Park, S.; Kim, K. P.; Huh, K. M.; Song, J.; Park, J. O.; Choi, E. Multifunctional Nanorobot System for Active Therapeutic Delivery and Synergistic Chemo-photothermal Therapy. *Nano Lett.* **2019**, *19* (12), 8550−8564.

(6) Sancho-Albero, M.; Encabo-Berzosa, M. D. M.; Beltrán-Visiedo, M.; Fernández-Messina, L.; Sebastián, V.; Sánchez-Madrid, F.; Arruebo, M.; Santamaría, J.; Martín-Duque, P. Efficient encapsulation of theranostic nanoparticles in cell-derived exosomes: leveraging the exosomal biogenesis pathway to obtain hollow gold nanoparticle-hybrids. *Nanoscale* **2019**, *11* (40), 18825−18836.

(7) Ma, Z.; Wan, H.; Wang, W.; Zhang, X.; Uno, T.; Yang, Q.; Yue, J.; Gao, H.; Zhong, Y.; Tian, Y.; Sun, Q.; Liang, Y.; Dai, H. A Theranostic Agent for Cancer Therapy and Imaging in the Second Near-infrared Window. *Nano Res.* **2019**, *12* (2), 273−279.

(8) Surekha, B.; Kommana, N. S.; Dubey, S. K.; Kumar, A. V. P.; Shukla, R.; Kesharwani, P. PAMAM Dendrimer As a Talented Multifunctional Biomimetic Nanocarrier for Cancer Diagnosis and Therapy. *Colloids Surf., B* **2021**, *204*, No. 111837.

(9) Jin, Z.; Nguyen, K. T.; Go, G.; Kang, B.; Min, H. K.; Kim, S. J.; Kim, Y.; Li, H.; Kim, C. S.; Lee, S.; Park, S.; Kim, K. P.; Huh, K. M.; Song, J.; Park, J. O.; Choi, E. Multifunctional Nanorobot System for Active Therapeutic Delivery and Synergistic Chemo-photothermal Therapy. *Nano Lett.* **2019**, *19* (12), 8550−8564.

(10) Ahmad, M. Z.; Rizwanullah, M.; Ahmad, J.; Alasmary, M. Y.; Akhter, M. H.; Abdel-Wahab, B. A.; Warsi, M. H.; Haque, A. Progress in Nanomedicine-based Drug Delivery in Designing of Chitosan Nanoparticles for Cancer Therapy. *Int. J. Polym. Mater. Polym. Biomater.* **2022**, *71* (8), 602−623.

(11) Xie, J.; Chen, K.; Huang, J.; Lee, S.; Wang, J.; Gao, J.; Li, X.; Chen, X. PET/NIRF/MRI triple functional iron oxide nanoparticles. *Biomaterials* **2010**, *31* (11), 3016−3022.

(12) Kedar, U.; Phutane, P.; Shidhaye, S.; Kadam, V. Advances in Polymeric Micelles for Drug Delivery and Tumor Targeting. *Nanomed.-Nanotechnol. Biol. Med.* **2010**, *6* (6), 714−729.

(13) Evers, A.; Krah, S.; Demir, D.; Gaa, R.; Elter, D.; Schroeter, C.; Zielonka, S.; Rasche, N.; Dotterweich, J.; Knuehl, C.; Doerner, A. Engineering Hydrophobicity and Manufacturability for Optimized Biparatopic Antibody−drug Conjugates Targeting c-MET. *mAbs* **2024**, *16* (1), No. 2302386.

(14) Pourjamal, N.; Yazdi, N.; Halme, A.; Joncour, V. L.; Laakkonen, P.; Saharinen, P.; Joensuu, H.; Barok, M. Comparison of trastuzumab emtansine, trastuzumab deruxtecan, and disitamab vedotin in a multiresistant HER2-positive breast cancer lung metastasis model. *Clin. Exp. Metastasis* **2024**, *41*, 91.

(15) Katrini, J.; Boldrini, L.; Santoro, C.; Valenza, C.; Trapani, D.; Curigliano, G. Biomarkers for Antibody−Drug Conjugates in Solid Tumors. *Mol. Cancer Ther.* **2024**, *23*, 436.

(16) Jäger, S.; Könning, D.; Rasche, N.; Hart, F.; Sensbach, J.; Krug, C.; Raab-Westphal, S.; Richter, K.; Unverzagt, C.; Hecht, S.; Anderl, J.; Schröter, C. Generation and Characterization of Iduronidase-Cleavable ADCs. *Bioconjugate Chem.* **2023**, *34* (12), 2221−2223.

(17) Li, H.; Huang, H.; Tan, H.; Jia, Q.; Song, W.; Zhang, Q.; Zhou, B.; Bai, J. Key processes in tumor metastasis and therapeutic strategies with nanocarriers: a review. *Mol. Biol. Rep.* **2024**, *51* (1), 1−9.

(18) Song, Y.; Du, Y.; Hu, C.; Lei, L.; Yang, L.; Wang, X.; Jiang, C.; Gao, H. Metformin-Mediated Immunosuppressive Microenvironment Remodeling in Combination with Chemotherapy via a Spatial-Specific Multi-Responsive Carrier-Free Self-Assembled Nanoparticle. *Adv. Funct. Mater.* **2024**, *34*, No. 2316145.

(19) Rana, A.; Adhikary, M.; Bhatnagar, S. "Smart" Drug Delivery: A Window to Future of Translational Medicine. *Front. Chem.* **2023**, *10*, No. 1095598.

(20) Drago, J. Z.; Modi, S.; Chandarlapaty, S. Unlocking the potential of antibody−drug conjugates for cancer therapy. *Nat. Rev. Clin. Oncol.* **2021**, *18* (6), 327−344.

(21) Kaplon, H.; Crescioli, S.; Chenoweth, A.; Visweswaraiah, J.; Reichert, J. M. Antibodies to Watch in 2023. *mAbs* **2023**, *15* (1), No. 2153410.

(22) Dumontet, C.; Reichert, J. M.; Senter, P. D.; Lambert, J. M.; Beck, A. Antibody-drug Conjugates Come of Age in Oncology. *Nat. Rev. Drug Discovery* **2023**, *22* (8), 641−661.

(23) Conilh, L.; Sadilkova, L.; Viricel, W.; Dumontet, C. Payload Diversification: a Key Step in the Development of Antibody-drug Conjugates. *J. Hematol. Oncol.* **2023**, *16* (1), 3.

(24) Fuentes-Antrás, J.; Genta, S.; Vijenthira, A.; Siu, L. L. Antibody-drug Conjugates: in Search of Partners of Choice. *Trends Cancer* **2023**, *9* (4), 339−354.

(25) Nguyen, T.; Bordeau, B. M.; Balthasar, J. P. Mechanisms of ADC Toxicity and Strategies to Increase ADC Tolerability. *Cancers* **2023**, *15* (3), 713.

(26) Pan, L.; He, Q.; Liu, J.; Chen, Y.; Ma, M.; Zhang, L.; Shi, J. Nuclear-Targeted Drug Delivery of TAT Peptide-Conjugated Monodisperse Mesoporous Silica Nanoparticles. *J. Am. Chem. Soc.* **2012**, *134* (13), 5722−5725.

(27) Kanamala, M.; Wilson, W. R.; Yang, M.; Palmer, B. D.; Wu, Z. Mechanisms and Biomaterials in pH-responsive Tumour Targeted Drug Delivery: A review. *Biomaterials* **2016**, *85*, 152−167.

(28) Han, H.; Hou, Y.; Chen, X.; Zhang, P.; Kang, M.; Jin, Q.; Ji, J.; Gao, M. Metformin-Induced Stromal Depletion to Enhance the Penetration of Gemcitabine-Loaded Magnetic Nanoparticles for Pancreatic Cancer Targeted Therapy. *J. Am. Chem. Soc.* **2020**, *142* (10), 4944−4954.

(29) Tian, H.; Yu, L.; Zhang, M.; He, J.; Sun, X.; Ni, P. Dextran-doxorubicin prodrug nanoparticles conjugated with CD147 monoclonal antibody for targeted drug delivery in hepatoma therapy. *Colloids Surf., B* **2023**, *228*, No. 113400.

(30) Lehot, V.; Neuberg, P.; Ripoll, M.; Daubeuf, F.; Erb, S.; Dovgan, I.; Ursuegui, S.; Cianférani, S.; Kichler, A.; Chaubet, G.; Wagner, A. Targeted Anticancer Agent with Original Mode of Action Prepared by Supramolecular Assembly of Antibody Oligonucleotide Conjugates and Cationic Nanoparticles. *Pharmaceutics* **2023**, *15* (6), 1643.

(31) Dudchak, R.; Podolak, M.; Holota, S.; Szewczyk-Roszczenko, O.; Roszczenko, P.; Bielawska, A.; Lesyk, R.; Bielawski, K. Click chemistry in the synthesis of antibody-drug conjugates. *Bioorg Chem.* **2024**, *143*, No. 106982.

(32) Zhang, H.; Zhang, Z.; Wang, X.; Wang, D.; Xu, H.; Liu, Z.; Zhang, X.; Tang, Z.; Chen, X. Preparation of Trastuzumab-DM1 Conjugate with a High Drug-to-Antibody Ratio for Breast Cancer Therapy. *Nano Today* **2024**, *54*, No. 102134.

(33) Matsui, Y.; Inomata, M.; Tojigamori, M.; Sonoda, K.; Shiraishi, N.; Kitano, S. Suppression of Tumor Growth in Human Gastric Cancer with HER2 Overexpression by an Anti-HER2 Antibody in a Murine Model. *Int. J. Oncol.* **2005**, *27* (3), 681−685.

(34) Xie, J.; Chen, M.; Zhou, J.; Mo, M.-S.; Zhu, L.-H.; Liu, Y.-P.; Gui, Q.-J.; Zhang, L.; Li, G.-Q. miR-7 Inhibits the Invasion and Metastasis of Gastric Cancer Cells by Suppressing Epidermal Growth Factor Receptor Expression. *Oncol. Rep.* **2014**, *31* (4), 1715−1722.

(35) Janjigian, Y. Y.; Viola-Villegas, N.; Holland, J. P.; Divilov, V.; Carlin, S. D.; Gomes-DaGama, E. M.; Chiosis, G.; Carbonetti, G.; de




https://doi.org/10.1021/acsomega.4c07442
*ACS Omega* 2024, 9, 48598−48606

Stanchina, E.; Lewis, J. S. Monitoring Afatinib Treatment in HER2-Positive Gastric Cancer with 18F-FDG and 89Zr-Trastuzumab PET. *J. Nucl. Med.* **2013**, *54* (6), 936−943.

(36) Ito, K.; Mitsunaga, M.; Arihiro, S.; Saruta, M.; Matsuoka, M.; Kobayashi, H.; Tajiri, H. Molecular targeted photoimmunotherapy for HER2-positive human gastric cancer in combination with chemotherapy results in improved treatment outcomes through different cytotoxic mechanisms. *BMC Cancer* **2016**, *16*, 37.

(37) Peng, Y.; Xu, Y.; Zhang, X.; Deng, S.; Yuan, Y.; Luo, X.; Hossain, M. T.; Zhu, X.; Du, K.; Hu, F.; Chen, Y.; Chang, S.; Feng, X.; Fan, X.; Ashktorab, H.; Smoot, D.; Meltzer, S. J.; Hou, G.; Wei, Y.; Li, S.; Qin, Y.; Jin, Z. A Novel Protein AXIN1−295aa Encoded by CircAXIN1 Activates the Wnt/$\beta$-catenin Signaling Pathway to Promote Gastric Cancer Progression. *Mol. Cancer* **2021**, *20* (1), 158.



https://doi.org/10.1021/acsomega.4c07442
*ACS Omega* 2024, 9, 48598−48606